

Structural features of CeO₂(111) revealed by dynamic SFM

S Gritschneider¹, Y Namai², Y Iwasawa² and M Reichling¹

¹ Fachbereich Physik, Universität Osnabrück, Barbarastraße 7, 49076 Osnabrück, Germany
² Department of Chemistry, University of Tokyo, Hongo, Bunkyo-ku, Tokyo 113-0033, Japan

E-mail: reichling@uos.de

Received 11 November 2004, in final form 23 November 2004

Published 11 January 2005

Online at stacks.iop.org/Nano/16/S41

Abstract

Cerium dioxide is an insulating material that is important in various fields of catalysis and often used as an oxygen reservoir. The (111) surface of CeO₂ is catalytically active and we study this surface in its various oxidation states by dynamic force microscopy, an analysis that may eventually help to establish structure–function relationships for catalysis. We present highly resolved images and atomic details of surface features on CeO₂(111) like terrace structures, step edges, kinks and hexagonally shaped pits that are naturally formed during surface preparation by sputtering and annealing cycles. We find that such structures can be well imaged with atomic resolution and that they exhibit morphological characteristics that are significantly different in details from those of cleaved CaF₂(111), a surface with exactly the same crystallographic structure and very similar lattice constants and ionic radii. In this study, we continuously monitor the shape of the tip apex and demonstrate that high quality atomic resolution imaging is possible with one tip, although the tip apex is drastically changed by wear during 45 h of scanning.

(Some figures in this article are in colour only in the electronic version)

1. Introduction

The rare earth oxide ceria has recently experienced increased attention for technical applications due to its unique catalytic properties [1–3]. The most prominent devices involving CeO₂ include the three-way catalyst [4–6], flue gas treatment in fuel cracking and solid oxide fuel cells [7, 8]. They utilize ceria's remarkable oxygen storage and diffusion capability [9]. This feature is strongly related to the facile creation, healing and diffusion of oxygen vacancies, especially at the surface.

For a deeper understanding of the diffusion processes, it is essential to study the surface at the atomic scale. Up to now, several studies have been published dealing with investigations of the CeO₂(111) surface by STM and dynamic SFM; they included the preparation of surfaces at different oxidation states and exposure of reduced surfaces to various gases [10–15]. Such studies can reveal important information about surface chemistry at the atomic level and provide important information for deducing structure–function relationships.

The present contribution is the first in a series of investigations where we aim for a very detailed understanding and eventually a quantitative interpretation of observed structures and atomic scale contrast formation in dynamic force microscopy imaging. While we focus here on highly resolved imaging of larger features like terrace structures, step edges, kinks and hexagonal pits found on the as-prepared CeO₂(111) surface, contrast formation for individual ions, point defects and small defect clusters will be discussed in further communications.

Our interest in CeO₂(111) also stems from its close structural relationship to CaF₂(111), the standard dielectric surface for atomically resolved dynamic SFM. Recognizing the identity in crystal structure and the strong similarity in lattice constants and ionic radii, we are interested in identifying similarities and differences in SFM contrast formation. While the basic observations in contrast formation appear to be very similar for both materials, a variety of additional structural features are found on CeO₂(111) that have not been observed on CaF₂(111).

An important issue in high resolution force microscopy is the detailed structure of the tip apex at the nanometre and atomic scales. To obtain quantitative information about the tip used in this study, we thoroughly characterized the tip during our experiments by regularly taking detuning-distance curves [16] and examining the tip apex before and after imaging with a scanning electron microscope.

2. Experimental details

Experiments were performed in a UHV chamber operated at a base pressure of 5×10^{-8} Pa. The system was equipped with a commercial dynamic scanning force microscope (SFM), a direct current heating stage, and an Ar⁺-ion-sputter source. Preparation of the polished CeO₂ sample ($5.5 \times 1.2 \times 0.95$ mm³, Commercial Crystal Laboratories) consisted of several cycles of Ar⁺-ion sputtering (1.5 keV, 3 min) and subsequent annealing at 1200 K, following a recipe published earlier [17]. A successful preparation yields stacks of hexagonal terraces and pits which appear flat down to the atomic level. The topography of a typical surface as shown in figures 1(a) and (b) is dominated by stacks of hexagonal pits and protrusions often interconnected by bridging terraces. The step height is a multiple of the O–Ce–O triple layer height (312 pm). We were aiming to prepare large terraces as the chance of achieving atomic resolution on a terrace increases with its size. By trial and error we found settings allowing a stable reproduction of best imaging conditions.

We scanned the surface with instrumentation and techniques as used in our earlier studies [18], and operated the dynamic force microscope in the constant-height mode which on flat terraces is easy to operate as it basically only involves one regulation circuit to keep the oscillation amplitude constant. Furthermore, this mode of operation avoids distortion of ionic contrast due to possible peculiarities of the distance regulation loop. Usually one would assume that the constant-detuning mode would be more suitable for imaging topographic features that are the topic of this contribution. However, this is often not the case as we experience in experimental practice and as can be understood by the following consideration. The constant-detuning mode requires a large gain in the distance regulation loop. The overall effect of the gain setting is determined, however, by two parameters, the loop gain itself and the scanning speed. The setting of the loop gain is limited to a certain level, above which strong regulation oscillations lead to distortions in the measurement process. Therefore, we have to use a slower loop that can principally be compensated by reducing the scanning speed. However, we find that slow scanning can also be detrimental to the measurement, due to thermal drift that is unavoidable for our room temperature SFM measurements. Best results are obtained for a scanning speed above 40 nm s^{-1} . As a compromise, allowing at the same time precise imaging of atomic contrast and with somewhat less precision larger topographic features, we apply the constant-height mode with a somewhat higher loop gain than usual. It is one goal of this contribution to demonstrate that by a sensitive choice of parameters like scanning speed, average detuning and loop gain, regulation artefacts can be minimized but, depending on the main focus of the study, this has to be adjusted for each individual measurement.

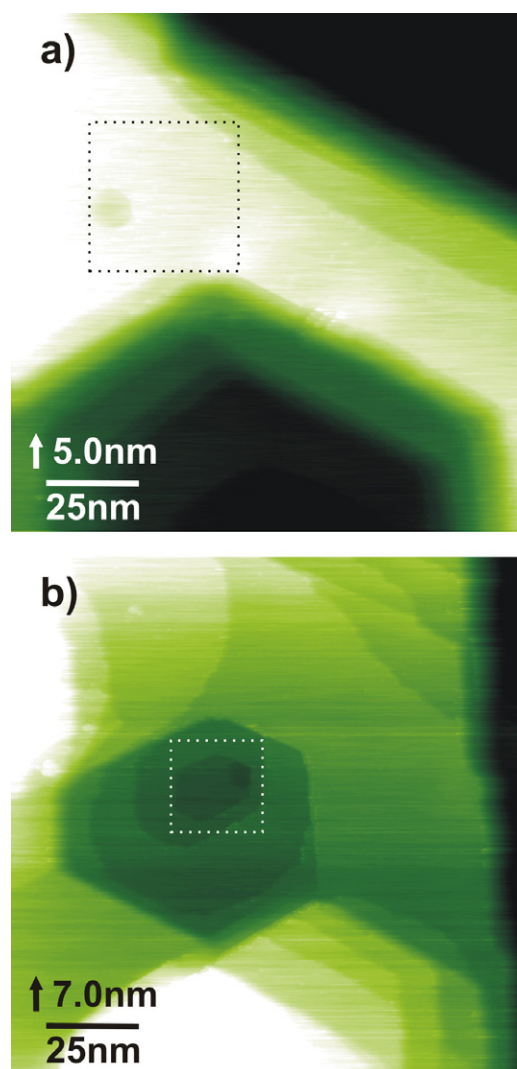


Figure 1. Typical surface morphology of the as-prepared CeO₂(111) surface. Stacks of terraces form hexagonally shaped nested pit and protrusion structures of some nanometres in height. The topmost terraces exhibit small flat pits and are often connected via narrow bridges. Magnified views of the square sections containing pits are shown in figure 7. $\Delta f_{\text{set}} = -4$ Hz (a) and -5 Hz (b), respectively.

For imaging we used commercial conductive silicon cantilevers with resonance frequencies of 60–70 kHz and spring constants of a few N m^{-1} . Q -values were above 20 000 in the UHV. The cantilever oscillation amplitudes were kept constant at a level of 30–40 nm.

All tips can be assumed to be covered with a native silicon oxide layer when purchased. We used these tips without further treatment like sputtering or flashing. For some experiments, however, we attached a carbon nanostructure at the tip apex. The length of those nanotips is some ten nanometres and the apex radius is typically some nanometres, in any case smaller than that of the silicon oxide tip [19]. Such carbon structures turned out to be very robust and allow measurements for extended periods with much less blunting of the tip than observed for conventional tips. While we recorded extended series of images with this tip, here we only present the results that are within the focus of this paper, namely frames from figures 5 and 6.

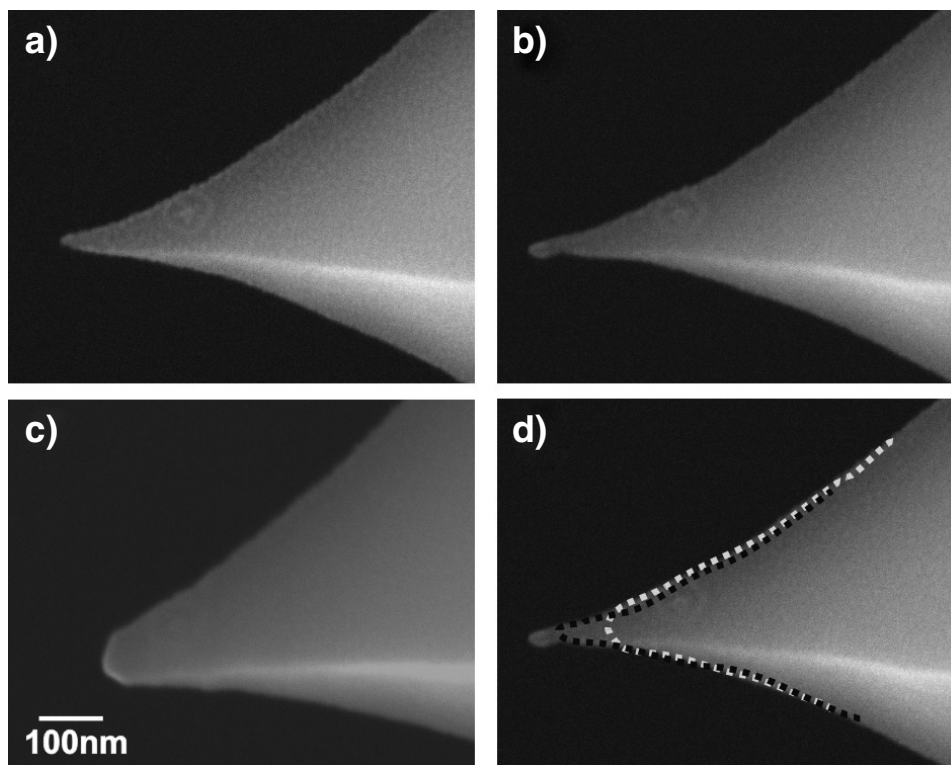


Figure 2. SEM images of a modified SFM tip. (a) Standard silicon tip covered with native oxide. (b) The same tip after electron beam assisted carbon deposition, and (c) after 45 h of measurement. (d) For a better comparison and demonstrating tip blunting, silhouettes from (a) to (c) are combined.

As a fully quantitative interpretation of atomic scale contrast formation involving theoretical modelling is the final goal of our studies, great care was taken to characterize the nanoscopic structure of the apex of some tips used. For this purpose, we were aiming to create a stable and well defined tip apex, and we examined its shape by scanning electron microscopy (SEM) before and after each series of experiments. This procedure is illustrated here for the example of an oxidized silicon tip extended by depositing carbon at the end. The lifecycle of such a carbon tip extension is illustrated in the series of SEM images shown in figure 2. Frame (a) shows the as-supplied oxidized silicon tip having a radius of about 10 nm, while frame (b) was taken immediately after depositing the tip extension in the SEM but prior to SFM measurements. The tip was examined in the SEM again after 45 h of SFM measurement, and the respective SEM micrograph is shown in frame (c). The superposition of the three images displayed in frame (d) demonstrates that, despite increased stability due to the carbon coverage, the tip was subject to considerable wear, reducing the tip length by 110 nm and increasing the tip radius to 25 nm.

This is in good agreement with detuning-distance curves that were taken after each measuring session; selected results are shown in figure 3. The onset of the Δf -curves, corresponding to the average detuning necessary for atomic resolution, tends to stronger detuning, i.e. to lower detuning values as a function of usage, while the slope of the detuning curve decreases, indicating stronger long-range forces. This is exactly the behaviour one would expect for a continuously blunting tip. During the entire period of measurements, we

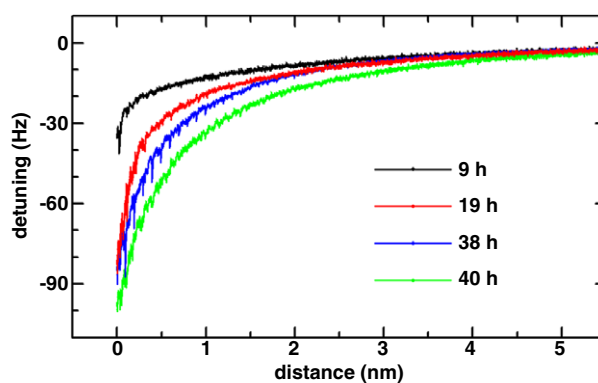


Figure 3. Detuning distance curves taken for the SFM tip from figure 2 at different stages of the measurement period specified in hours of usage during a period of 16 days. The onset and the slope of the curves decrease monotonously during extensive measurements, strongly indicating a blunting of the tip. Highest resolution experiments were possible at any time after formation of a suitable nanotip by interaction with the surface.

were able to record high quality atomic resolution images, although this became increasingly difficult with time. During this time, we repeatedly formed a nanotip at the tip apex by accidentally or deliberately picking up or dropping material from/to the surface. We anticipate that these nanotips determine the atomic contrast while the tip apex influences imaging stability via long-range interaction forces. When the tip becomes blunt, long-range forces dominate and imaging may become unstable due to the formation of multiple tip-surface interactions.

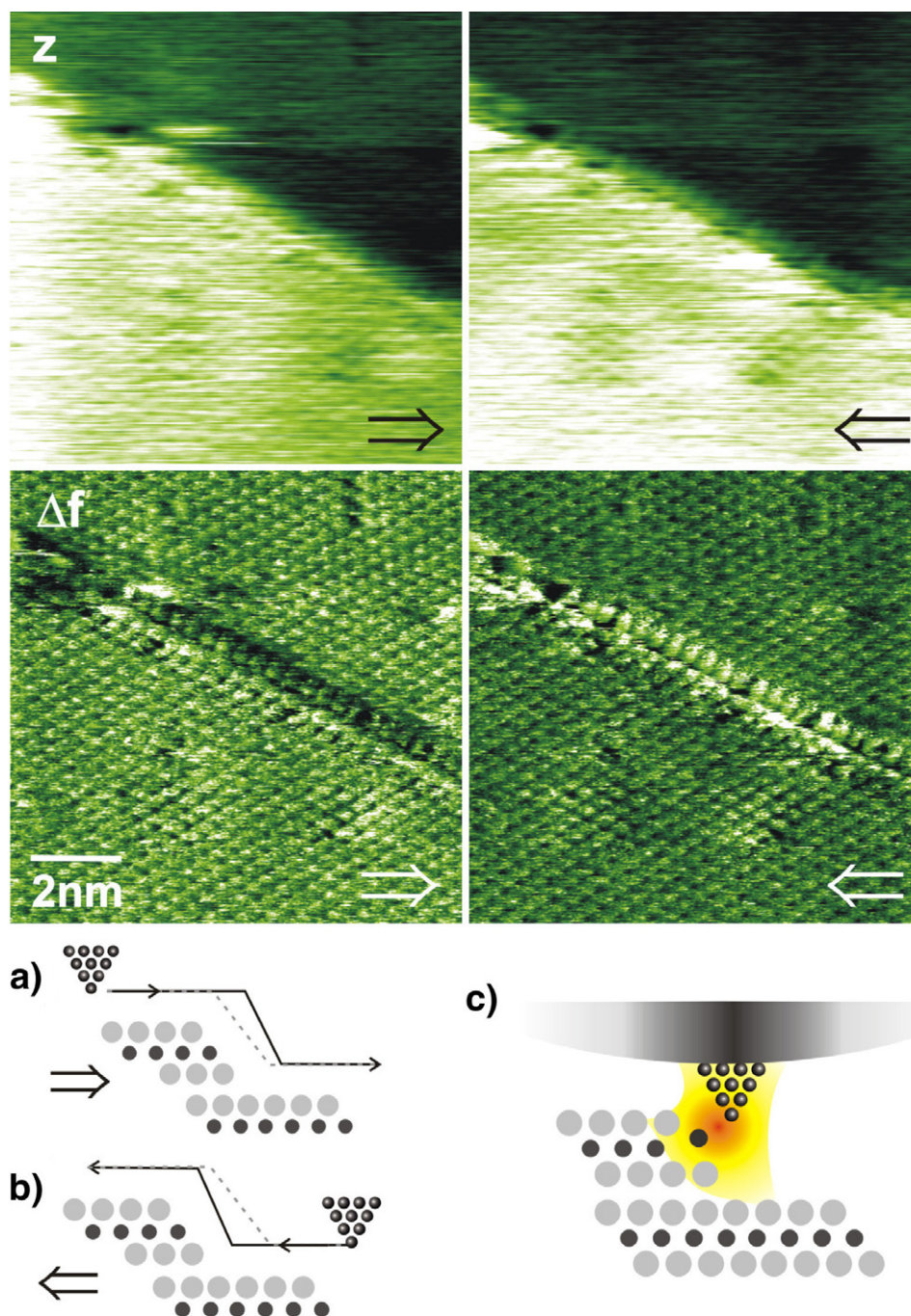


Figure 4. Images demonstrating atomic resolution at a step edge of one triple-layer step height. Topographic (top) and detuning (bottom) signals recorded in forward (\Rightarrow) and backward (\Leftarrow) scanning directions reproduce the step structure and artefacts discussed in the body of the text. The contrast enhancement at edge ions is explained by a combination of artefacts illustrated in schematics (a) and (b). Schematic (c) illustrates proposed relaxation processes at the step edge. $\Delta f_{\text{set}} = -15$ Hz.

3. Results and discussion

Once the surface is well prepared, it is straightforward to obtain atomic resolution on flat terraces. The periodicity of the perfect lattice as well as single point defects and small defect clusters can be well resolved. Some of these results are shown in figures 4–7; however, their detailed discussion and interpretation will be topic of a forthcoming publication. Here we focus on atomic resolution imaging at step edges, kinks and nanometre-sized pit defects found on the as-prepared

surface. As a first example in figure 4, atomic resolution on two different terraces separated by a triple-layer step is demonstrated. We simultaneously recorded the topography (top) and detuning (bottom) signals in forward (left) and backward (right) scanning direction. To compensate for the change at the step edge, the gain of the z -feedback loop was set to 2%, a slightly higher set point compared to standard constant height measurements performed on flat terraces, where the loop-gain is below 1%. Furthermore, the scanning speed was reduced to 45 nm s^{-1} , corresponding to a very slow

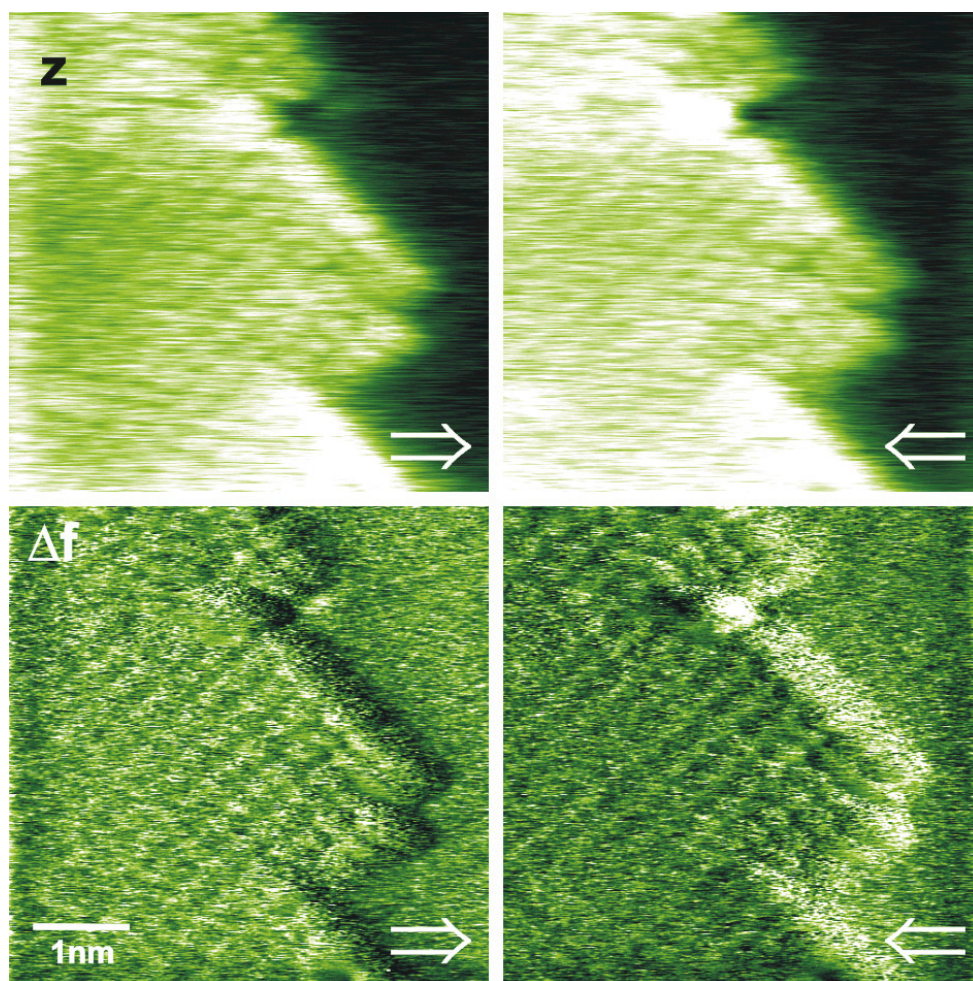


Figure 5. Topography (z) and detuning (Δf) signals in forward (\Rightarrow) and backward (\Leftarrow) scanning directions of a triple-layer step with several kinks. Edge ions are only faintly visible due to increased regulation effects close to the step edge. The bright contrast feature at the upper kink may represent an adsorbed molecule. $\Delta f_{\text{set}} = -50$ Hz.

scanline acquisition rate of 1.5 lines s^{-1} , compared to up to 10 lines s^{-1} used in usual constant height measurements (the percentage value for the loop-gain is arbitrary and provides only comparative information). While these settings allow us to scan securely across the edge, the distance regulation is now fast enough also to follow the atomic corrugation on the terraces. Obviously a residual contrast in the topography is the price to pay, if atomic contrast in the detuning image throughout the entire frame is desired. This unwanted side effect has to be taken into account for the interpretation of the image as it may induce artefacts, which again can be identified by comparing forward and backward direction scans. One good example of a scanning artefact can be recognized here in imaging the edge. In the forward direction the edge ions appear very dark, while they are very bright in the backward direction. Sketches (a) and (b) from figure 4 suggest the reason for this discrepancy. In the forward direction the tip cannot follow the edge contour (dashed line) but it takes some time for the regulation to accommodate to the topography (full line). This results in less interaction at the step edge and, hence, a darker shading. For the backward direction exactly the opposite is the case. The regulation cannot retract the tip fast enough, so the tip is too close to the surface, leading to stronger interaction

indicated by a brighter shading. However, despite this artefact, we still notice that in both scanning directions two rows of ions at the edge appear brighter and larger than the other ions, and as this is true for both scanning directions it is a real physical effect and not due to any scanning artefact. A close inspection of the topography signal exhibits that the edge is not an abrupt step, but there is an intermediate contrast corresponding to the right edge atoms in the detuning frames. Assuming an oxygen terminated surface, a possible interpretation of this phenomenon is that the intermediate ions are cerium ions which are not covered by oxygen ions at the step edge, and therefore they exhibit strong relaxation as suggested by the sketch 4(c). The second row of ions appearing larger would then be the last completely shielded row of cerium ions of the top terrace. For a more detailed discussion and interpretation of these contrast patterns, we refer to forthcoming publications based on experimental and theoretical studies that are presently performed.

It is very interesting, of course, to zoom further into a step edge to obtain a more detailed view of the individual ions. However, we realize that for scanning smaller frames we cannot maintain the scanning speed at a high value, but have to reduce it to yield stable imaging conditions. The

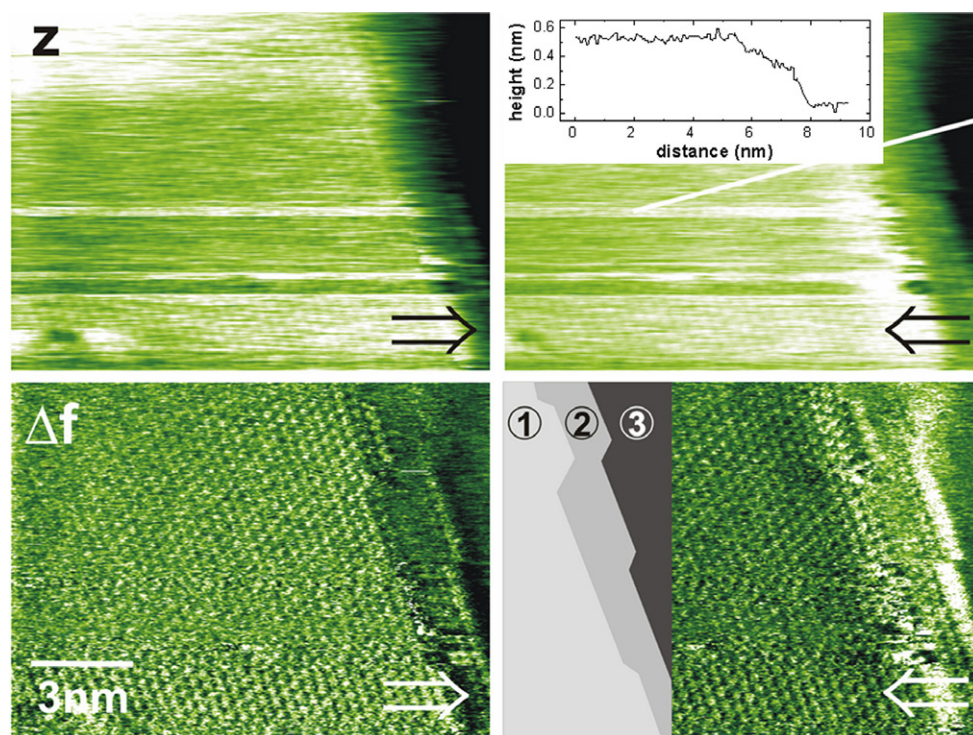


Figure 6. Topography (z) and detuning (Δf) signals in forward (\Rightarrow) and backward (\Leftarrow) scanning directions of a double step structure. Terraces on the as-prepared $\text{CeO}_2(111)$ surfaces are often found to have a width of only a few atoms. The inset in the lower right frame shows the structural details of the double-step structure. Instabilities at kink sites often result in image distortions and tip changes as apparent by stripes along the fast scanning direction. $\Delta f_{\text{set}} = -83$ Hz.

$7 \times 7 \text{ nm}^2$ frames shown in figure 5, for example, are recorded at a scanning speed of only 28 nm s^{-1} and with a similar loop gain as before. Therefore, the effective gain of the regulation is increased and the step can be seen very clearly in the topographic image with some edge ions appearing brighter. But in the detuning image the step induced scanning artefact described before is much more intense. While in the forward direction some edge ions still appear somewhat brighter, in the backward direction atomic details are completely overruled by the artefact. The intermittent ions seen in figure 4 are not visible. This was the best result we could obtain from a test of various imaging conditions, and we conclude that small frames are very difficult to be recorded in the constant-height mode at room temperature. Nonetheless, this image is very interesting as it shows an edge with a multitude of kinks, which is a typical appearance on $\text{CeO}_2(111)$. At the upper kink we observed an even higher contrast enhancement than at the others. Possibly this is due to an adsorbate, as kinks are favourable adsorption sites for small molecules from the residual gas.

While the above-described step structures are well known from imaging $\text{CaF}_2(111)$ [18], in figure 6 we introduce a new formation, namely double steps forming terraces of only a few atomic rows in width. The image was taken with similar settings as in figure 4. Three height levels are clearly distinguished in the topographic frames, where atomic contrast was achieved on differently shaped upper and middle terraces which excludes that this structure is simply an artefact due to a double tip. The inset gives a schematic drawing of terrace formation as it is not so easy to identify from a single frame. The three terraces are numbered and have been given different

grey values. The height profile across the steps does not clearly resolve the intermediate step, but the total height difference between the upper and lower terrace is 0.6 nm , which again proves that this structure is real and not a double-tip effect. At the lower part of the frames, where still only two terraces are scanned, imaging is very much comparable to the situation in figure 4. Atomic resolution in the detuning signal is obtained on both terraces and step ions are enhanced. Regulation leads to a darker appearance in the forward direction and a brighter appearance in the backward direction. However, as the third terrace comes into play, it becomes increasingly difficult to maintain atomic contrast. Scanning across kinks sometimes induces instabilities leading to horizontal stripes in the signals. Due to these peculiarities, it is extremely hard to obtain atomic resolution on three levels when the middle terrace is very narrow.

Flat pits on terraces are a common feature on $\text{CeO}_2(111)$ that has never been observed on $\text{CaF}_2(111)$. In figure 7 we show examples to discuss such pit structures. The frames additionally exhibit stable point defects, some of them aligned at the periphery of a pit. For the discussion of these defects and their dynamics, however, we refer to a forthcoming paper. In figure 7(a) we present results from a detail taken from the typical bridge terrace shown in figure 1(a) that has a width of 30 nm at the narrowest point. Here, the scanning speed was 150 nm s^{-1} and the loop gain set to 16%. While most atomic details are not distinguishable any more in all signals, atomic rows are still clearly visible in the detuning signal, and both edges exhibit several kinks yielding enhanced contrast. For better discrimination between the terraces, they are numbered

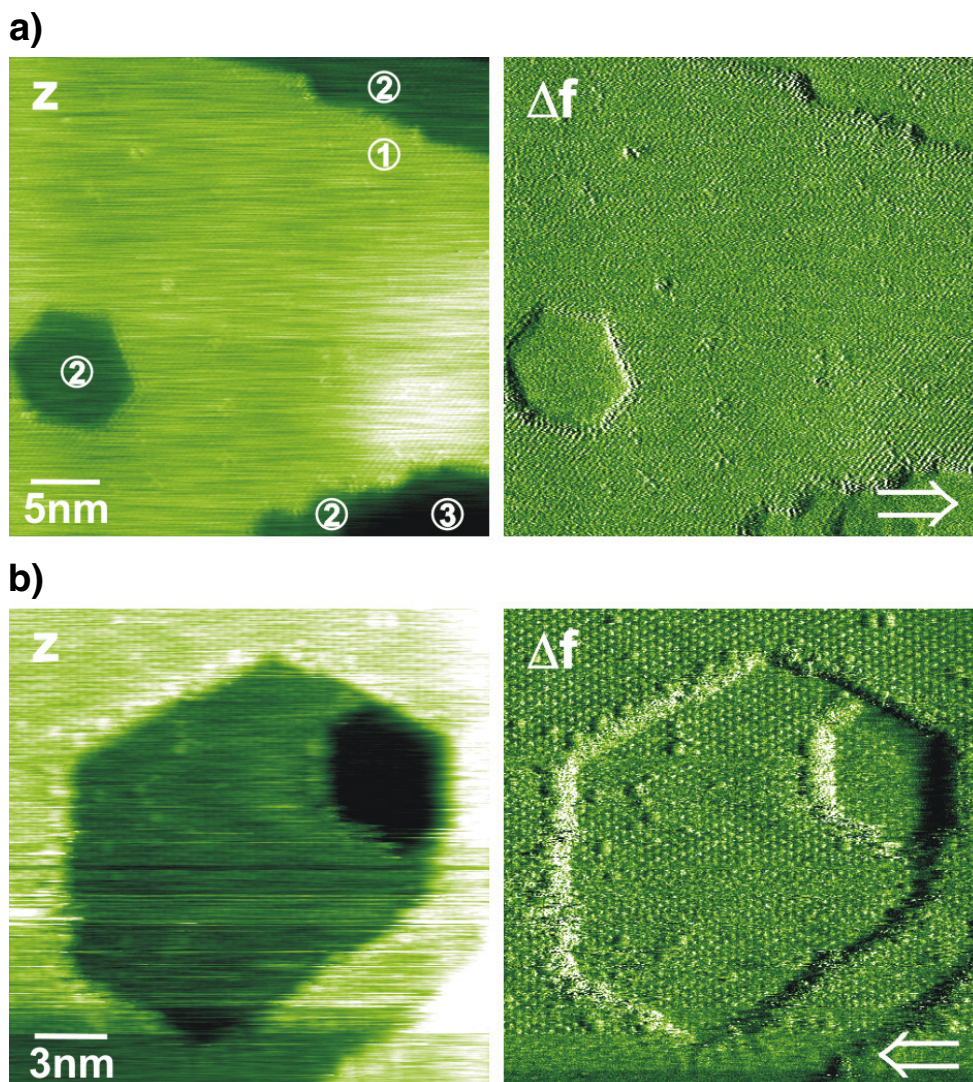


Figure 7. The frames are enlarged views of corresponding images of figure 1. (a) Topography (z) and detuning (Δf) signals of a bridge with a shallow pit scanned at a speed of 150 nm s^{-1} and a loop gain of 16% for stable imaging at larger scales. Atomic rows are only faintly visible on terraces but are well resolved at step edges. Terraces are labelled corresponding to their topographic height. $\Delta f_{\text{set}} = -4 \text{ Hz}$. (b) While the depth of small hexagonal pits consisting of fewer than 15 atoms per edge is one triple-layer as shown above, larger pits appear as terraced structures of nested pits. Four different height levels are distinguishable in the backward topographic scan. Atomic resolution on four different terraces within the same frame was achieved in the detuning signal. $\Delta f = -5 \text{ Hz}$.

according to their topographic height. Besides some point-like defects the dominant surface feature is a hexagonal pit embedded in the terrace. This structure is almost perfectly symmetric and has edges consisting of 10–13 atoms. Such pits appear randomly on the surface and we found that the depth of small pits, i.e. those with less than 15 atoms per edge, is one triple-layer height, while larger pits often appear in terraced structures of nested pits as demonstrated in figure 7(b), that is an enlarged view of the feature shown in figure 1(b). The edges of the larger pit consist of 16–26 atoms and those of the inner pit have about 6–9 atoms. The topographic frame provides information about the different height levels, but, recorded with a scanning speed of 60 nm s^{-1} and a loop gain of 7%, the image barely exhibits any atomic corrugation. However, the corresponding detuning image carries the full atomic corrugation information from all four height levels involved, except in the lower part of the frame, where contrast

was established by a tip change induced by the interaction of the tip with a kink site. In this measurement we aimed for atomic resolution on as many different height levels as possible. Therefore, the parameters were optimized to follow the topography very quickly, without losing contrast in the detuning. In fact, the atomic contrast is comparable and of high quality on all height levels. The edges, however, are not well resolved as all atomic information is covered by dark and bright regulation artefacts extending over 1 nm. Figures 7(a) and (b) are instructive examples to demonstrate how the scanning parameters have to be chosen to obtain good resolution at step edges or on terraces. Imaging with such high resolution is very susceptible to tip changes, and we found that they often appear at the same kink sites when repetitively scanning the same pit sites. In this frame, imaging conditions were unusually stable so that only for some scan lines was the measuring process slightly disturbed.

4. Conclusions

The CeO₂(111) surface is most interesting to be studied by dynamic scanning force microscopy. It yields a strong ionic contrast with distinct patterns and exhibits a variety of nanoscale features that are a challenge and test for the imaging capability of the force microscope. This study revealed the overall morphology of the surface dominated by hexagonally shaped features and details of the atomic structure at edges and kinks separating terraces by one triple-layer of O–Ce–O and regularly formed pits appearing as single pits with a triple-layer depth or nested structures of pits spanning a height range of several triple-layers. The observed features can be anticipated to represent thermodynamically stable or at least meta-stable structures as the apparent surface morphology is a result of annealing the surface to high temperature. This morphology appears to be distinctly different from that of CaF₂(111) prepared by cleavage and heated to similarly high temperatures, although there is almost quantitative agreement between the ionic structure and size parameters between both crystals. Hence, this study clearly reveals the different bonding properties of CeO₂ compared to the strongly ionic CaF₂ that also manifest themselves in surface point-like defects and the high mobility of oxygen on the surface that will be elucidated in detail in a forthcoming study.

Acknowledgments

The authors are indebted to A L Shluger (having initiated this work) and A Foster for most stimulating discussions as well as T Arai for preparing and characterizing the carbon modified tips used in some of the experiments presented here.

Financial support by the Deutsche Forschungsgemeinschaft and the Stiftung Volkswagenwerk is gratefully acknowledged.

References

- [1] Trovarelli A, de Leitenburg C, Boaro M and Dolcetti G 1999 *Catal. Today* **50** 353–67
- [2] Bernal S, Kaspar J and Trovarelli A 1999 *Catal. Today* **50** 173
- [3] Trovarelli A 1996 *Catal. Rev.-Sci. Eng.* **38** 439–520
- [4] Gandhi H S, Graham G W and McCabe R W 2003 *J. Catal.* **216** 433–42
- [5] Wu X D, Xu L H and Weng D 2004 *Appl. Surf. Sci.* **221** 375–83
- [6] Yao H C and Yao Y F Y 1984 *J. Catal.* **86** 254–65
- [7] Shao Z P and Haile S M 2004 *Nature* **431** 170–3
- [8] Hibino T, Hashimoto A, Inoue T, Tokuno J, Yoshida S and Sano M 2000 *Science* **288** 2031–3
- [9] He H, Dai H and Au C T 2004 *Catal. Today* **90** 245–54
- [10] Nörenberg H and Briggs G A D 1997 *Phys. Rev. Lett.* **79** 4222–5
- [11] Namai Y, Fukui K-I and Iwasawa Y 2004 *Nanotechnology* **15** 49–54
- [12] Namai Y, Fukui K-I and Iwasawa Y 2003 *J. Phys. Chem. B* **107** 11666–73
- [13] Fukui K-I, Takakusagi S, Tero R, Aizawa M, Namai Y and Iwasawa Y 2003 *Phys. Chem. Chem. Phys.* **5** 5349–59
- [14] Fukui K-I, Namai Y and Iwasawa Y 2002 *Appl. Surf. Sci.* **188** 252–6
- [15] Nörenberg H and Briggs G A D 1999 *Surf. Sci.* **424** L352–5
- [16] Barth C, Foster A S, Reichling M and Shluger A L 2001 *J. Phys.: Condens. Matter* **13** 2061–79
- [17] Namai Y, Fukui K-I and Iwasawa Y 2003 *Catal. Today* **85** 79–91
- [18] Barth C and Reichling M 2000 *Surf. Sci.* **470** L99–103
- [19] Arai T, Gritschneider S, Tröger L and Reichling M 2004 *Nanotechnology* **15** 1302–6